Energy and Power Engineering, 2026, 18(9), 586-613
https://www.scirp.org/journal/epe
ISSN Online: 1947-3818
ISSN Print: 1949-243X

Numerical Simulation Study on In-Furnace Combustion Characteristics of 29 MW Industrial Pulverized Coal Boiler

Leikai Deng[1], Tinghui Huang[1], Rong Yan[2], Zhongyan Wang[3], Xin Zhang[2]*

[1]Hubei Chibi Electric Power Co., Ltd., Chibi, China
[2]School of Energy Science and Engineering, Harbin Institute of Technology, Harbin, China
[3]Beijing Yelian Technology Co., Ltd., Beijing, China
Email: *2057769574@qq.com

How to cite this paper: Deng, L.K., Huang, T.H., Yan, R., Wang, Z.Y. and Zhang, X. (2026) Numerical Simulation Study on In-Furnace Combustion Characteristics of 29 MW Industrial Pulverized Coal Boiler. *Energy and Power Engineering*, **18**, 586-613.
https://doi.org/10.4236/epe.2026.189027

Received: July 3, 2026
Accepted: September 4, 2026
Published: September 7, 2026

Abstract

To clarify the in-furnace combustion characteristics of a 29 MW industrial pulverized coal hot-water boiler using centrally fuel-rich swirl combustion technology, a full-scale numerical model of the boiler furnace and burner was established and validated against industrial test data. The effects of the separated secondary air ratio and flue gas recirculation ratio on the flow field, temperature distribution, gas-species distribution, NO_X formation, and furnace outlet parameters were investigated under full-load conditions. The validation results showed that the average deviation between the simulated and measured flue gas temperatures in the burner region was 9.8%, and the deviations in furnace outlet O_2 concentration, NO_X concentration, and combustible content in fly ash were 1.0%, 10.5%, and 11.3%, respectively, indicating that the numerical model was reliable. The results showed that the separated secondary air ratio significantly affected the central recirculation zone, flame morphology, and combustion completeness. Excessively high or low separated secondary air ratios were unfavorable for stable combustion and burnout, whereas a separated secondary air ratio of 55.4% produced a more reasonable high-temperature-zone distribution and more uniform furnace heating. Increasing the flue gas recirculation ratio shifted the central recirculation zone upward, reduced the high-temperature-zone area and flame filling degree, weakened coal burnout, and decreased NO_X emissions. When the flue gas recirculation ratio was 30%, the NO_X concentration and flue gas temperature at the furnace outlet decreased by 19% and 31 K, respectively, while the O_2 concentration and combustible content in fly ash increased by 0.55 and 12.03 percentage points, respectively. Overall, the optimal separated secondary air ratio was 55.4%; the flue gas recirculation ratio should be controlled below 20% when boiler efficiency and burnout are prioritized, and above 25% when NO_X reduction is the primary objective.

Keywords

Industrial Pulverized Coal Boiler, Centrally Fuel-Rich Swirl Combustion, Numerical Simulation, Separated Secondary Air, Flue Gas Recirculation, NO_X Emissions

1. Introduction

Industrial boilers are important energy-conversion equipment for heating, steam supply, and industrial production, and they play a significant role in China's energy consumption and pollutant-emission system. Coal-fired industrial boilers are widely used and large in number. During operation, they emit NO_X, SO_2, smoke, and dust, which have significant impacts on the ecological environment and human health [1]-[4]. In recent years, with increasingly strict requirements for boiler energy conservation and environmental protection, some key regions have imposed more stringent ultra-low-emission standards for newly built coal-fired boilers. Therefore, coal-fired industrial boilers urgently need to achieve low NO_X emissions while maintaining combustion efficiency and safe operation [5]-[7].

Compared with chain-grate boilers and circulating fluidized bed boilers, industrial pulverized coal boilers have the advantages of high thermal efficiency, high automation level, flexible start-up and shutdown, and strong potential for pollutant control [8]-[10]. However, existing industrial pulverized coal boilers still suffer from high initial NO_X emissions, local slagging in the pre-combustion chamber and furnace, and high unburned carbon content in fly ash [11]-[13]. To solve these problems, researchers have carried out extensive studies on burner-structure optimization, air staging, flue gas recirculation, and swirl-stabilized combustion. Previous studies have shown that rational secondary-air organization, enhanced in-furnace recirculation, and improved mixing between pulverized coal and air are important approaches for improving coal burnout and reducing NO_X formation [14]-[18].

The centrally fuel-rich swirl combustion technology feeds high-concentration primary air-pulverized coal flow into the central recirculation zone of the burner, allowing pulverized coal to ignite and burn in a high-temperature, low-oxygen, and strongly reducing atmosphere. This combustion organization can simultaneously improve flame stability, burnout, and NO_X suppression [19]-[21]. When this technology is applied to industrial boilers, the coupling among flow, heat transfer, combustion, and pollutant formation becomes more complex because of the small furnace size, limited number of burners, and frequent load fluctuations. Therefore, industrial tests alone cannot provide complete information on the velocity field, temperature field, and species-concentration distribution inside the furnace.

Numerical simulation is necessary to further analyze the effects of combustion-organization parameters [21] [22].

In this study, a 29 MW industrial pulverized coal hot-water boiler using centrally fuel-rich swirl combustion technology is selected as the research object. A full-scale numerical model of the furnace and burner is established, and the reliability of the model is verified by comparison with industrial test results. On this basis, the effects of separated secondary air ratio and flue gas recirculation ratio on the in-furnace flow structure, temperature distribution, O_2/CO/NO_X concentration distributions, and furnace-outlet parameters are investigated. The influence mechanisms of different operating parameters on stable combustion, burnout, slagging risk, and NO_X emission control are clarified, providing a basis for optimizing the operation of centrally fuel-rich swirl combustion technology in industrial pulverized coal boilers.

However, a full-scale and industrially validated understanding is still limited regarding how separated secondary-air redistribution and flue-gas recirculation jointly regulate the recirculation structure, flame filling, burnout, wall-adjacent atmosphere, and NO_X formation in centrally fuel-rich swirl industrial boilers. Therefore, the novelty of the present work lies in a plant-validated parametric and mechanistic assessment that links the internal flow and combustion fields with directly usable operating windows for separated secondary air and flue-gas recirculation.

2. Methods

2.1. Numerical Simulation of Combustion

Firstly, 1:1 scale geometric model of the 29 MW hot water boiler prototype was created using 3D modeling software. Subsequently, the grid division work was completed using a grid division software. As shown in **Figure 1**, the extraction section for the calculation results in this chapter is the longitudinal cross-section of the furnace passing through the center of the over burner, marked by the red line in the figure. Each part of the calculation domain was divided into structured grids to improve grid quality, accelerate convergence, and be closer to the actual model. At the same time, different processing methods were adopted for the grids in different areas: 1) The existence of axial bending blades makes the drainage areas formed by the secondary air inside and outside the burner relatively complex, and it is not suitable to model and divide this part of the drainage area together with the furnace. Therefore, during the operation, this part of the complex drainage area was modeled and divided separately; 2) The number of secondary air channels in the burner separation is large, and it is not suitable to model and divide each nozzle separately on the furnace. Therefore, the secondary air separation channels were also modeled and divided separately; 3) In the calculation domain with complex flow fields and concentrated combustion, a denser node distribution was arranged, while the remaining parts were arranged with a relatively sparse node distribution based on the computing capacity.

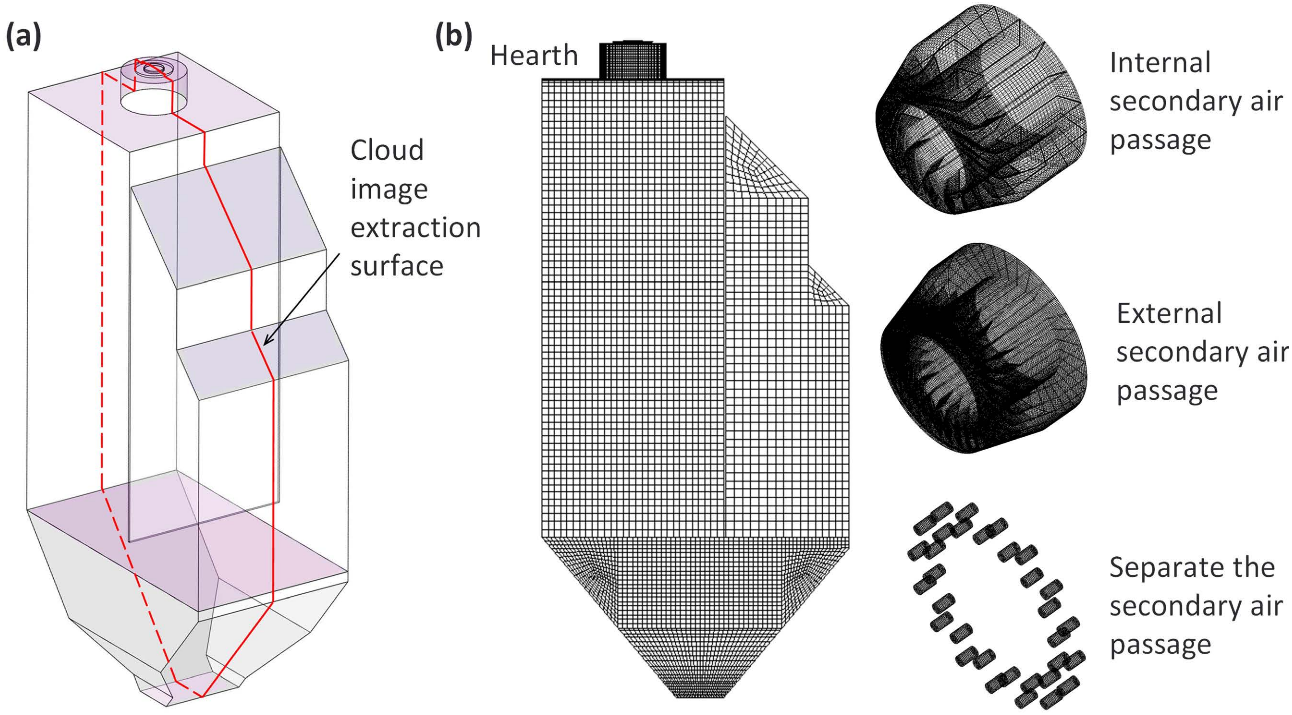

Figure 1. Schematic diagram of the geometric model and meshing division of computing domain diagram. (a) Geometric model and cloud map extraction surface; (b) Mesh generation.

Under the condition that all other factors remain the same, the grid independence verification is conducted solely by adjusting the node distribution within the computational domain. The aim is to enhance the accuracy of the calculation results and avoid interference from the grid quality of the computational domain on the calculation results. As shown in **Figure 2(a)**, when the number of grids is 200,000, the axial velocity along the centerline is significantly different from that under other grid numbers. When the number of grids increases to 600,000, the axial velocity along the centerline changes slightly. To further verify the sensitivity of the calculation results to the node distribution, the calculated results of the average oxygen content and temperature at the furnace outlet were extracted for comparison. As shown in **Figure 2(b)**, when the number of grids increases from 200,000 to 1,000,000, the average oxygen content at the furnace outlet gradually increases, and the average temperature at the furnace outlet gradually decreases. When the number of grids increases from 800,000 to 1,000,000, the average oxygen content and temperature at the furnace outlet change slightly. Considering the reliability and speed of the calculation, the final number of grids adopted in this chapter is 800,000. Quantitatively, increasing the grid number from 0.8 to 1.0 million changes both the furnace-outlet O_2 concentration and temperature by less than approximately 0.3%, confirming that the 0.8-million-cell grid is sufficiently grid-independent for the present comparative analysis.

The inlet of each stage of the air supply channel for the burner adopts a velocity inlet boundary condition. The parameters of each inlet are calculated based on the design parameters of the prototype, and the turbulence intensity is set at 10%.

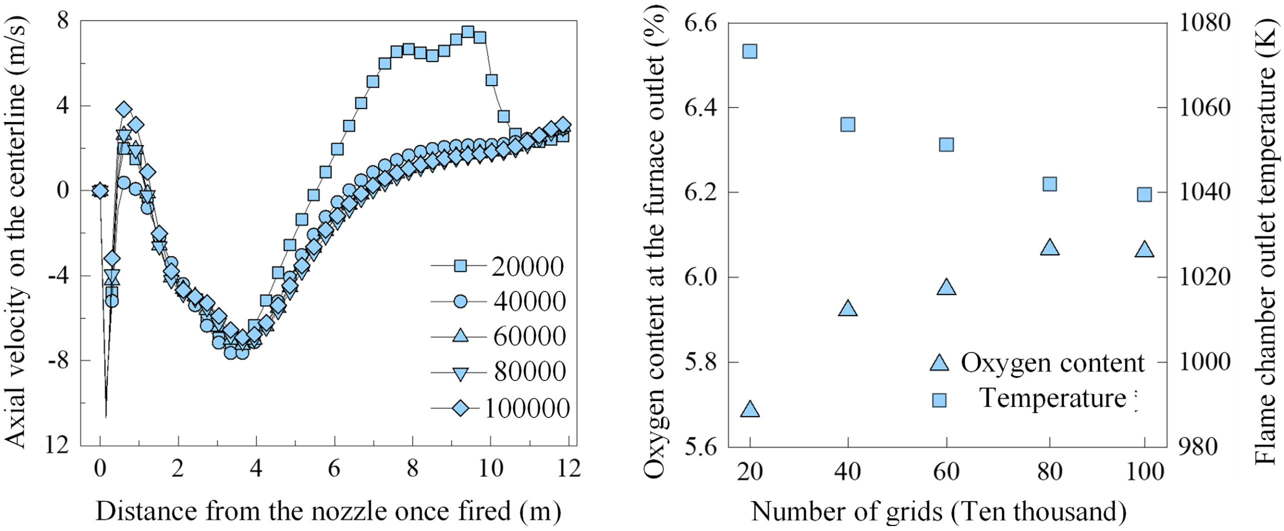

Figure 2. Grid independence verification.

The slip coefficient between the primary air and the coal powder particles is taken as 0.8. The particle size of the coal powder is in accordance with the Rosin-Ramler distribution. The outlet of the boiler furnace adopts a pressure outlet boundary, and the static pressure at the outlet is set at −50 Pa. During the calculation, the SIMPLE algorithm, which is widely used in computational fluid dynamics, is adopted for solving. After achieving a certain degree of cold-state convergence of the flow field, the thermal state calculation is carried out.

The gas-phase turbulence was modeled using the Realizable k-ε model ($C1\varepsilon = 1.44$, $C2 = 1.90$, $\sigma k = 1.0$, and $\sigma\varepsilon = 1.2$), while pulverized-coal particles were treated as a discrete phase with stochastic/random-trajectory tracking. Radiative heat transfer was described using the P-1 model. Volatile release was represented by the two-competing-rates devolatilization model with $\alpha 1 = 0.3$ and $\alpha 2 = 1.0$, $A1 = 1.13 \times 10^5\ s^{-1}$, $E1 = 5.64 \times 10^7\ J{\cdot}mol^{-1}$, $A2 = 6.48 \times 10^{11}\ s^{-1}$, and $E2 = 1.74 \times 10^8\ J{\cdot}mol^{-1}$. Volatile combustion was solved using the species-transport/eddy-dissipation model with a two-step global reaction scheme, and char oxidation was described by the kinetic/diffusion model with a pre-exponential factor of 0.0034 and an activation energy of $9.65 \times 10^7\ J{\cdot}mol^{-1}$. NO_X was evaluated in post-processing. Thermal NO was calculated using the extended Zeldovich mechanism and fuel NO using the De-Soete mechanism, while prompt NO was neglected. For fuel-nitrogen partitioning, 90% of volatile nitrogen was assigned to HCN and 10% to NH3, and the char-N-to-NO conversion fraction was set to 0.1.

All investigated cases employed the same coal type, fuel-related properties, and Rosin-Rammler particle-size distribution; therefore, fuel properties were not treated as variables in the present parametric study. The devolatilization kinetic parameters listed above were applied consistently to all cases. Because the complete original coal-characterization dataset and detailed Rosin-Rammler distribution parameters were not retained in the archived model documentation, no retrospectively reconstructed values are reported. Accordingly, the present study focuses on the relative effects of separated secondary-air redistribution and flue-gas recirculation under an identical fuel basis, and the quantitative conclusions are limited to the investigated coal and operating conditions. The same wall thermal treatment was retained for all simulated cases, and radiative heat transfer was treated using the P-1 model. The detailed numerical values of the original wall thermal settings (prescribed wall temperature or heat flux and wall emissivity) were not retained in the archived model documentation; therefore, no estimated values are introduced. Consequently, the comparative trends among operating conditions are emphasized, whereas absolute wall-temperature and heat-transfer predict.

2.2. Model Validation

To verify the reliability of the numerical simulation, numerical calculations were conducted for the operating condition with an inner secondary air door opening of 20%. **Figure 3** shows the temperature results of the burner area obtained by the two methods. Through analysis, it can be seen that the temperature distribution patterns obtained from the industrial test and the numerical simulation are basically consistent, especially after a certain distance from the measurement starting point. However, there are also certain differences: the temperature distribution of the flue gas near the bottom of the pre-combustion chamber shows that the simulated value is slightly lower than the measured value, while the temperature of the flue gas near the outlet of the pre-combustion chamber shows that the simulated value is slightly higher than the measured value. The average deviation between the flue gas temperature obtained from the test and the simulation is 9.8%. **Table 1** presents the results of the furnace outlet parameters obtained by the two methods. Through comparative analysis, it can be seen that the furnace outlet parameters obtained from the industrial test and the numerical simulation are the same in quantity. The deviations between the outlet O_2 concentration, NO_X emission concentration, and combustible content in the fly ash obtained by the two methods are 1.0%, 10.5%, and 11.3%, respectively. In addition, the CO emission concentration obtained from the test is 7.6 ppm, while the result obtained from the simulation approaches 0 ppm. The near-zero simulated CO concentration, compared with the measured value of 7.6 ppm, is therefore regarded as a limitation in the prediction of trace-level CO rather than as evidence of close agreement. Nevertheless, the model reproduces the main quantities used in this study with reasonable accuracy, including the burner-region temperature and the outlet O_2 concentration, NO_X concentration, and combustible content in fly ash. Accordingly, the model is considered adequate for evaluating comparative trends in flow, temperature, burnout, and NO_X among the investigated operating conditions, while quantitative prediction of very low CO concentrations should be interpreted with caution.

The burner-region temperature validation shown in **Figure 3** contains 10 axial measurement locations from 0 to 900 mm from the measurement starting position, at approximately 100 mm intervals. These measurement points were used to obtain the reported mean temperature deviation of 9.8%. The available industrial-test record contains the reported measurement series but does not provide independent replicate datasets or sufficient instrument information for a rigorous retrospective uncertainty analysis. Therefore, no estimated uncertainty has been assigned, and this limitation is considered when interpreting the validation results.

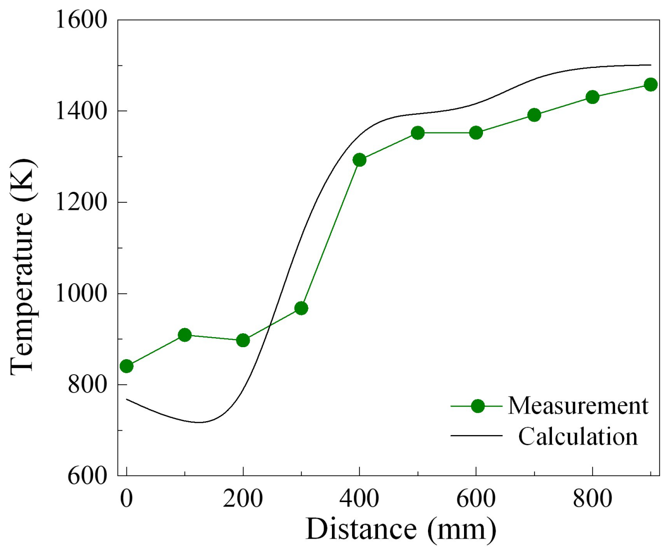

Figure 3. Comparisons of flue gas temperature in burner area between numerical and industrial test.

Table 1. Comparisons of furnace outlet results between numerical and industrial test.

Project	O_2 concentration (%)	CO concentration (ppm)	Fly ash C content (%)	NO_X (mg/m^3@O_2 = 9%)
Commercial	10.1	7.6	10.56	285.5
Simulation	10.0	3.5×10^{-7}	9.37	315.6

2.3. Separation Secondary Air Rate

The separated secondary-air ratio, R_{sep}, is defined on a total fresh-air mass-flow basis as $R_{sep} = m_{sep}/(m_{PA} + m_{ISA} + m_{OSA} + m_{sep}) \times 100\%$, where m_{PA}, m_{ISA}, m_{OSA}, and m_{sep} denote the mass flow rates of primary air, inner secondary air, outer secondary air, and separated secondary air, respectively. Recirculated flue gas is not included in this fresh-air denominator.

Firstly, the 29 MW hot water boiler adopting the central powder feeding swirl combustion technology of industrial coal powder boilers was selected as the research object. Numerical calculations were conducted on the combustion characteristics inside the boiler under different secondary air separation rates at the rated working condition. A total of six sets of working conditions were set up, with the secondary air separation rates being 85.7%, 71.4%, 55.4%, 42.9%, 28.6%, and

14.3%. The numerical simulation parameters are shown in **Table 2**. Under each working condition, the primary air volume, coal feeding volume, and total air volume remained unchanged, while the proportion of the separated secondary air continuously decreased, and the inner and outer secondary air volumes increased proportionally according to the area ratio.

Table 2. Simulation parameters under different rates of separated secondary air.

Project	Separated secondary air rate					
	85.7%	71.4%	55.4%	42.9%	28.6%	14.3%
Amount of primary air (kg/s)	0.52					
Internal secondary air volume (kg/s)	0.30	0.69	1.11	1.47	1.87	2.26
External secondary air volume (kg/s)	1.29	3.00	4.85	6.43	8.14	9.85
Separate the secondary air volume (kg/s)	12.63	10.53	8.26	6.32	4.21	2.11
Air temperature (K)	287.15					
Coal supply volume (kg/s)	1.56					

2.4. Flue Gas Recirculation Rate

The research of many scholars has confirmed that introducing tail-end flue gas into the circulation is an effective method to reduce NO_X emissions from boilers. However, when too much circulating flue gas enters the furnace, it will not only reduce the boiler efficiency but also affect the stable operation of the boiler. In this section, through numerical calculation methods, a thermodynamic simulation was conducted on the flow, combustion, and NO_X generation characteristics inside the furnace when a 29 MW hot water boiler operates at full load under different flue gas recirculation rates. **Table 3** presents the numerical simulation parameters under different flue gas recirculation rates. A total of 5 working conditions were set, with the flue gas recirculation rate being 0%, 15%, 20%, 25%, and 30%. In each working condition, the proportion of air volume in each level of air remains unchanged. The recirculating flue gas is mixed in the secondary air and the separated secondary air according to the area ratio and then sprayed into the furnace together with the air. Due to the introduction of low-temperature circulating flue gas absorbing more heat in the furnace, the coal feeding amount and the total air volume calculated by thermodynamic calculation will increase slightly. In the original numerical setup, Rre was prescribed directly as the operating flue-gas-recirculation parameter at 0%, 15%, 20%, 25%, and 30%. For all FGR cases, the fresh-air distribution among the air registers was maintained, while recirculated flue gas at 393.15 K was introduced through the outer secondary-air and separated secondary-air streams according to their respective flow-area proportions. Increasing Rre therefore increased the total gas flow through these two passages without changing the prescribed fresh-air distribution. Because the separate recirculated-flue-gas mass-flow values were not retained in the original reported dataset, they are not retrospectively reconstructed here.

Table 3. Simulation parameters under different ratios of recirculation flue gas.

Project	Flue gas recirculation rates				
	0%	15%	20%	25%	30%
Amount of primary air (kg/s)			0.52		
Internal secondary air volume (kg/s)			1.11		
External secondary air volume (kg/s)	4.85	4.85	4.85	4.86	4.86
Separate the secondary air volume (kg/s)	8.26	8.26	8.27	8.27	8.27
Air temperature (K)			287.15		
Circulating flue gas temperature (K)			393.15		
Coal supply volume (kg/s)	1.56	1.56	1.56	1.57	1.57

3. Results and Discussion

3.1. Separation Secondary Air Rate

Figure 4 shows the axial velocity distribution under different separation rates of secondary air at the hot state. In the hot-state axial velocity distribution diagram, the direction of the burner jet is taken as the positive direction. The airflow at the rear of the furnace is ejected in the opposite direction to the burner jet, so the axial velocity in this part is displayed as a negative value. When the separation rate of secondary air is 85.7%, only a small annular recirculation zone is formed in the premixing chamber, and no central recirculation zone can be formed in the furnace. The primary air-coal powder flow directly rushes out of the premixing chamber downward. At the same time, the primary air-coal powder flow in the furnace maintains a high axial velocity and rushes upward in parallel with the two separated secondary air jets. When the separation rate of secondary air is reduced to 71.4%, a central recirculation zone is formed in the furnace, but due to the small momentum of the secondary air, its carrying capacity for the primary air-coal powder flow is weak, and the recirculation zone is asymmetrically distributed. When the separation rate of secondary air is reduced to 28.6% to 55.4%, the recirculation zone is in the form of "droplets". At this time, the momentum of the secondary air is large, and it drives the airflow in the premixing chamber to rotate rapidly. The length and axial velocity of the central recirculation zone in the furnace increase as the separation rate of secondary air decreases, and more smoke flows back to the burner nozzle area. However, when the separation rate of secondary air is 14.3%, a large amount of airflow is ejected from the premixing chamber, and the axial velocity near the outlet of the premixing chamber increases rapidly. The high-speed airflow in the premixing chamber rushes upward and hinders the smoke reflux, causing the diameter and length of the central recirculation zone to significantly decrease. These results indicate that the recirculation structure is governed by a competition between swirl-induced entrainment and axial jet penetration: an excessively high separated-secondary-air fraction weakens the swirling-secondary-air momentum, whereas an excessively low fraction strengthens the outlet jet and suppresses the upstream development of the central recirculation zone.

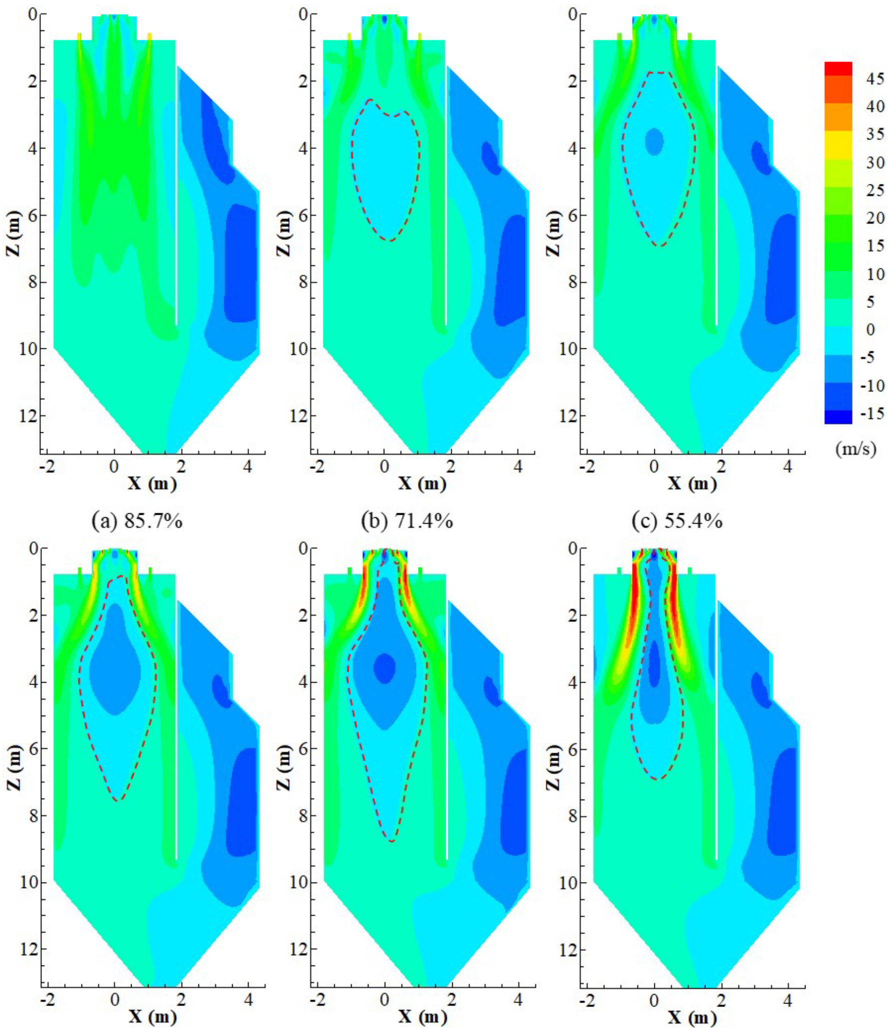

(a) 85.7% (b) 71.4% (c) 55.4% (d) 42.9% (e) 28.6% (f) 14.3%

Figure 4. Axial velocity contours in the furnace at different separated secondary-air ratios.

Figure 5 shows the velocity vector diagram when the separation secondary air rate is 14.3%. Near the outlet of the premix chamber, the axial velocity of the airflow also increases as the separation secondary air rate decreases. The airflow turns upward and moves forward in the cold ash hopper, entering the ascending furnace. Due to the influence of inertia, the axial velocity of the airflow is greater near the rear wall side in the ascending furnace.

Figure 6 shows the distribution of flue gas temperature under different secondary air separation rates. At the bottom of the pre-combustion chamber, the flue gas temperature is relatively low. This low-temperature zone can protect the wall of the pre-combustion chamber and is conducive to preventing the occurrence of high-temperature slagging on the wall of the pre-combustion chamber. Near the

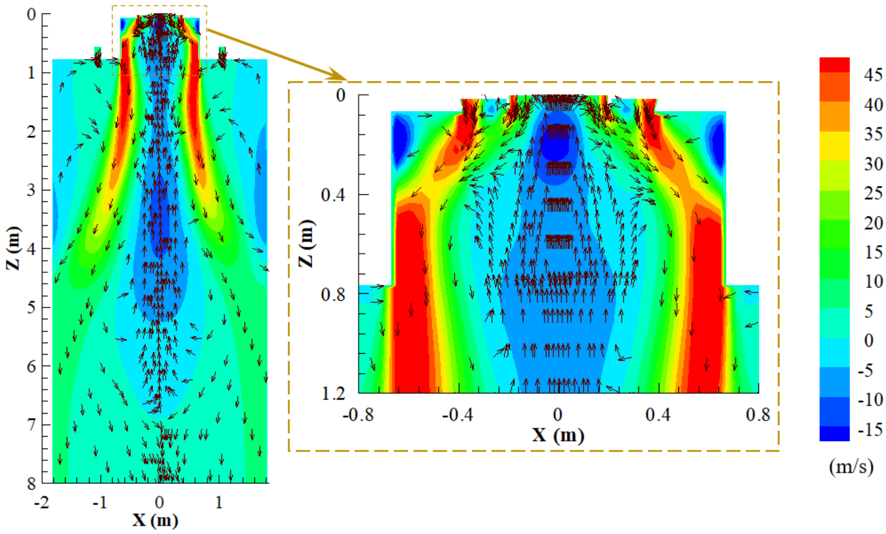

Figure 5. Velocity vector diagram when the rate of separated secondary air is 14.3%.

outlet of the secondary air separation, compared with the high-temperature flue gas in the furnace, the secondary air separation is supplied as cold air, with a lower temperature. Therefore, the movement trajectory of the secondary air separation in the furnace can be inferred based on the distribution of flue gas temperature in the furnace. Along the radial direction of the burner, the secondary air separation first deviates towards the center of the furnace after leaving the nozzle, and then gradually expands outward. Along the axial direction of the burner, as the secondary air separation rate decreases, the air volume gradually decreases, while the airflow rotation ability gradually increases, causing the mixing speed of the secondary air separation to gradually increase and the downward penetration distance to gradually shorten. As supplementary air, the purpose of the secondary air separation is to enhance the air stratification in the furnace. Premature mixing will weaken the degree of stratification.

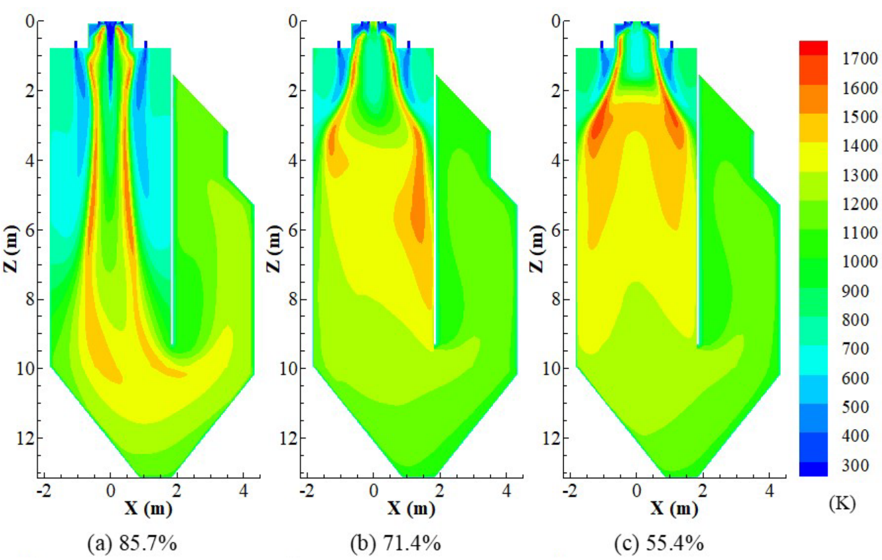

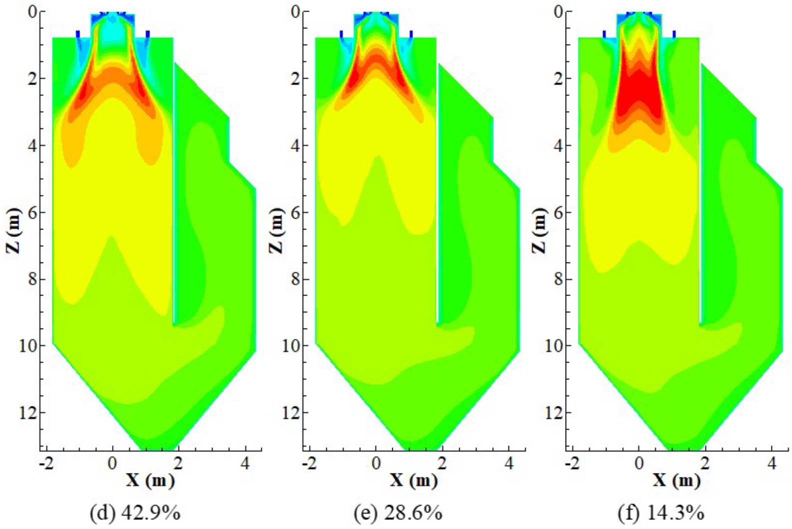

Figure 6. Furnace temperature contours at different separated secondary-air ratios.

The stable existence of the central recirculation zone can provide the necessary heat for the continuous combustion of pulverized coal, and is crucial for the ignition and stable combustion of the swirling pulverized coal burner. When the separation of secondary air rate is 85.7%, the airflow rotation is weak and cannot form a central recirculation zone to draw back the high-temperature flue gas. At this time, it is not conducive to the combustion of pulverized coal, and the temperature of the flue gas in the furnace is lower. Since the separation of secondary air has a certain distance in the radial direction from the outlet of the pre-combustion chamber, after losing the suction effect of the gas flow in the pre-combustion chamber, the separation of secondary air weakens the wrapping effect of the gas flow on the outlet of the pre-combustion chamber. From the temperature distribution, it can be seen that there is a sudden expansion of the high-temperature zone near the outlet of the pre-combustion chamber, which is not conducive to preventing the occurrence of high-temperature slagging near the outlet of the pre-combustion chamber. In addition, when the separation of secondary air rate is 85.7%, due to the weak airflow rotation ability, the airflow maintains a large downward impulse, and the high-temperature flue gas is pushed to the cold ash hopper area, which is prone to cause high-temperature corrosion and slagging in the cold ash hopper area. When the separation of secondary air rate is 71.4%, the temperature distribution in the downflow section of the furnace shows a significant asymmetry, that is, asymmetric combustion. The fundamental reason for this is the deviation of the flow field near the outlet of the pre-combustion chamber. Asymmetric combustion causes the high-temperature flue gas to directly wash the water-cooled wall, which not only leads to the occurrence of high-temperature corrosion and slagging, but also poses a threat to the safe operation of the boiler. In conclusion, in order to ensure the safety of the boiler, the separation of secondary air rate should be set below 71.4%. Thus, the temperature response is directly coupled to the flow structure: stronger recirculation transports high-temperature combustion products back toward the burner to promote ignition, whereas excessive axial penetration shifts the high-temperature region downstream and reduces flame filling.

Figure 7 presents the area of the high-temperature zone within the furnace (the area on the cloud map extracted in Figure 6 where the temperature exceeds 1400 K) and the temperature distribution along the centerline of the furnace under different separation secondary air rates. When the separation secondary air rate is set at 14.3%, the area of the high-temperature zone and the highest flue gas temperature along the furnace centerline increase significantly. However, due to the compression from the high-speed pre-combustion chamber airflow, the flame is more difficult to expand outward and becomes a slender cylindrical shape. The filling degree of the flame in the furnace is insufficient, which is not conducive to the complete combustion of the coal powder. When the separation secondary air rate is between 28.6% and 55.4%, as the separation secondary air rate increases, the separation secondary air continuously enhances its ability to carry the high-temperature flue gas within the furnace upward, resulting in an increasing area of the high-temperature zone within the furnace, a gradually lower position of the high-temperature zone along the furnace centerline, and an increasing highest flue gas temperature. The increase and downward shift of the high-temperature zone area indicate that as the separation secondary air rate increases, the down-pushing depth of the coal powder flame gradually increases, and the residence time of the coal powder particles in the high-temperature zone also increases, which is beneficial for the complete combustion of the coal powder. When the separation secondary air rate is 55.4%, the high-temperature zone area is large, which is conducive to the complete combustion of the coal powder; the temperature along the furnace centerline rises more slowly, the position of the highest temperature peak is farther from the furnace top wall, and the highest temperature is also lower. The heating within the furnace is more uniform, which is beneficial for preventing slagging in the upper part of the furnace and avoiding local excessive high temperature leading

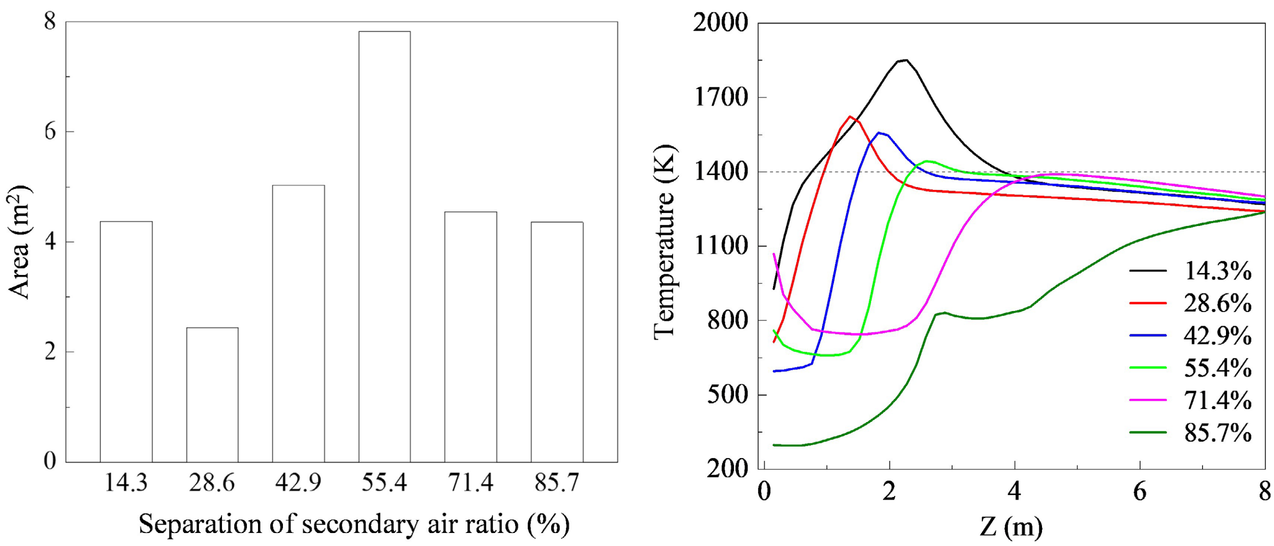

Figure 7. Effect of separated secondary-air ratio on high-temperature-zone area and furnace-centerline temperature.

to a large amount of NO_X generation. In conclusion, it is recommended to set the separation secondary air rate at around 55.4%.

Figure 8 shows the O_2 concentration distribution under different separation secondary air rates. The primary air pulverized coal flow ignites rapidly in the pre-combustion chamber, consuming a large amount of O_2, resulting in a significant gradient of O_2 concentration along the axial direction in the pre-combustion chamber. In the pre-combustion chamber, as the separation secondary air rate increases, the coal ignition occurs earlier, and the combustion in the pre-combustion chamber becomes more intense. The high O_2 concentration area at the bottom of the pre-combustion chamber gradually shrinks. In the high-temperature zone within the furnace and the area surrounded by the high-temperature zone, the O_2 concentration is lower. From the distribution of O_2 concentration within the central recirculation zone, it can be seen that the O_2 concentration is low at the center of the recirculation zone, which is not conducive to the combustion of coal powder. Therefore, the high-temperature zone appears at the edge

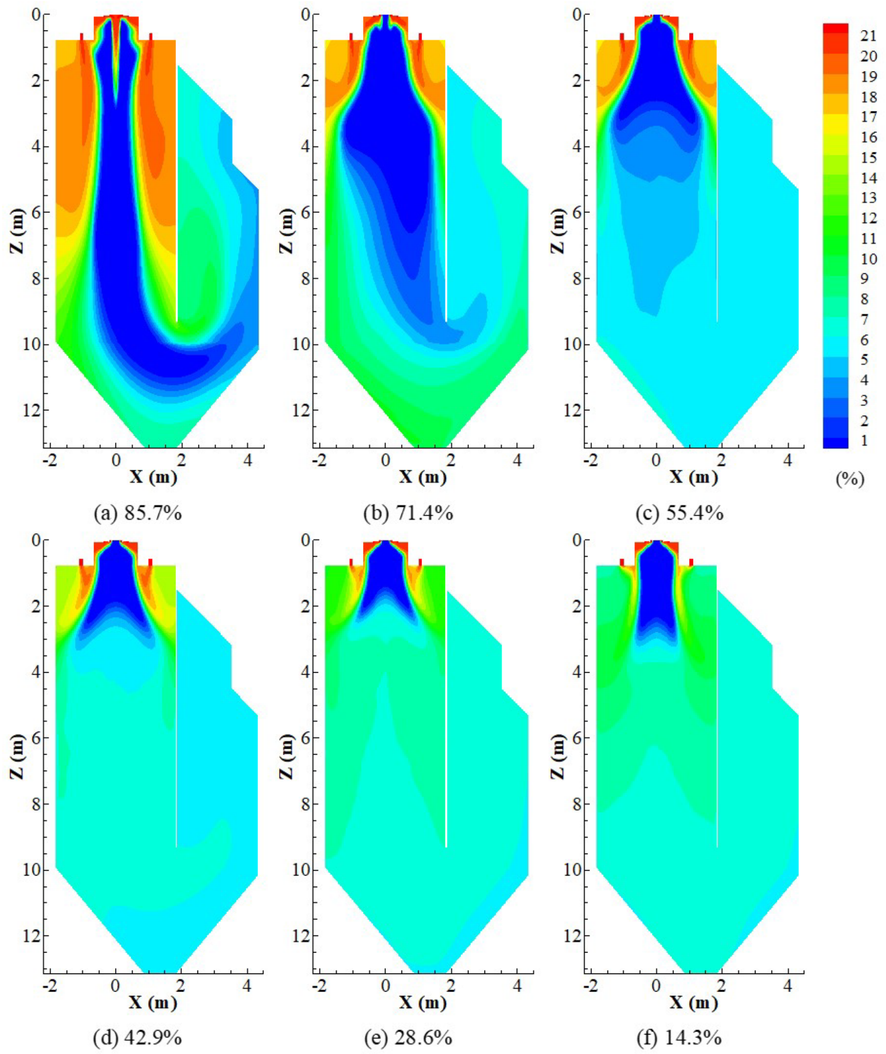

Figure 8. O_2 concentration contours at different separated secondary-air ratios.

of the recirculation zone. Here, both the recirculating high-temperature flue gas within the recirculation zone provides heat, and O_2 can be promptly replenished from the outside to support combustion. The O_2 distribution in the down-fired furnace well reflects the mixing process of the airflow in the pre-combustion chamber and the separated secondary air. Under the wrapping of the separated secondary air, the O_2 concentration near the water-cooled wall surface is relatively high, and the oxidizing atmosphere is conducive to preventing the occurrence of slagging on the wall surface. As the proportion of the separated secondary air decreases, the mixing of the separated secondary air and the airflow in the pre-combustion chamber accelerates, and the O_2 concentration near the side wall of the down-fired furnace gradually decreases. The area of the high O_2 concentration region between the separated secondary air and the water-cooled wall decreases, and the protective effect of the separated secondary air on the water-cooled wall weakens.

When the proportion of the separated secondary air is 85.7%, the primary air-coal powder flow gradually burns and consumes O_2 during the downward impulse process, forming a narrow and long low O_2 concentration area in the center of the down-fired furnace and the cold ash hopper. The momentum of the separated secondary air is large, and the down-fired furnace water-cooled wall area forms a large area of high O_2 concentration region, which well protects this area of water-cooled wall. After passing through the cold ash hopper, the low O_2 concentration area reaches the rear wall area of the up-fired furnace, which is prone to cause slagging on the wall surface of the up-fired furnace. When the proportion of the separated secondary air is 71.4%, due to the deviation of combustion, the O_2, CO and NO_X concentrations in the furnace are all deviated, and a low O_2, strong reducing atmosphere is formed near the down-fired furnace water-cooled wall, increasing the possibility of slagging on the side wall. When the proportion of the separated secondary air is 28.6% to 55.4%, the low O_2 concentration area in the center of the furnace rapidly shrinks. When the proportion of the separated secondary air is 14.3%, the diameter of the low O_2 concentration area in the center of the furnace shrinks and the length increases. In the pre-combustion chamber, as the proportion of the separated secondary air decreases, the coal powder ignition is advanced, and the combustion in the pre-combustion chamber is more intense. The high O_2 concentration area at the bottom of the pre-combustion chamber gradually shrinks. Meanwhile, as the proportion of the separated secondary air decreases, the O_2 concentration near the side wall of the down-fired furnace gradually decreases.

Figure 9 shows the distribution of CO concentration under different separation secondary air rates. When the separation secondary air rate is 85.7%, the airflow rotation ability is weak, and at the same time, the distance between the primary air coal powder flow and the separated secondary air flow is far. The mixing between the two parallel jets is slow, the separated secondary air is not replenished in time, and the coal powder combustion is incomplete, resulting in a large area of high CO concentration region in the furnace. When the separation secondary air rate is between 28.6% and 71.4%, as the separation secondary air rate decreases, the mixing of the separated secondary air accelerates, the air stratification degree weakens, the high CO region in the furnace significantly shrinks, the reducing atmosphere weakens, which is not conducive to the inhibition of NO_X generation, but at the same time, the high CO concentration region gradually moves away from the water-cooled wall, which can avoid the occurrence of high-temperature corrosion and slagging near the water-cooled wall. When the separation secondary air rate is 14.3%, a large amount of rotating secondary air quickly sucks in the primary air coal powder flow and high-temperature flue gas. The coal powder quickly ignites and burns in the pre-combustion chamber, and a large amount of CO is accumulated in the pre-combustion chamber, causing the CO concentration in the pre-combustion chamber to significantly increase. Although the coal powder quickly ignites in the pre-combustion chamber, the external separated secondary air is not replenished in time, resulting in a large amount of CO accumulation in the furnace, which is consumed slowly and directly affects the complete combustion of the coal powder. The CO field therefore reflects the competition between air staging and mixing: delayed oxygen replenishment preserves a reducing atmosphere but can impair burnout, while faster secondary-air mixing consumes CO more rapidly at the expense of weaker fuel-rich staging.

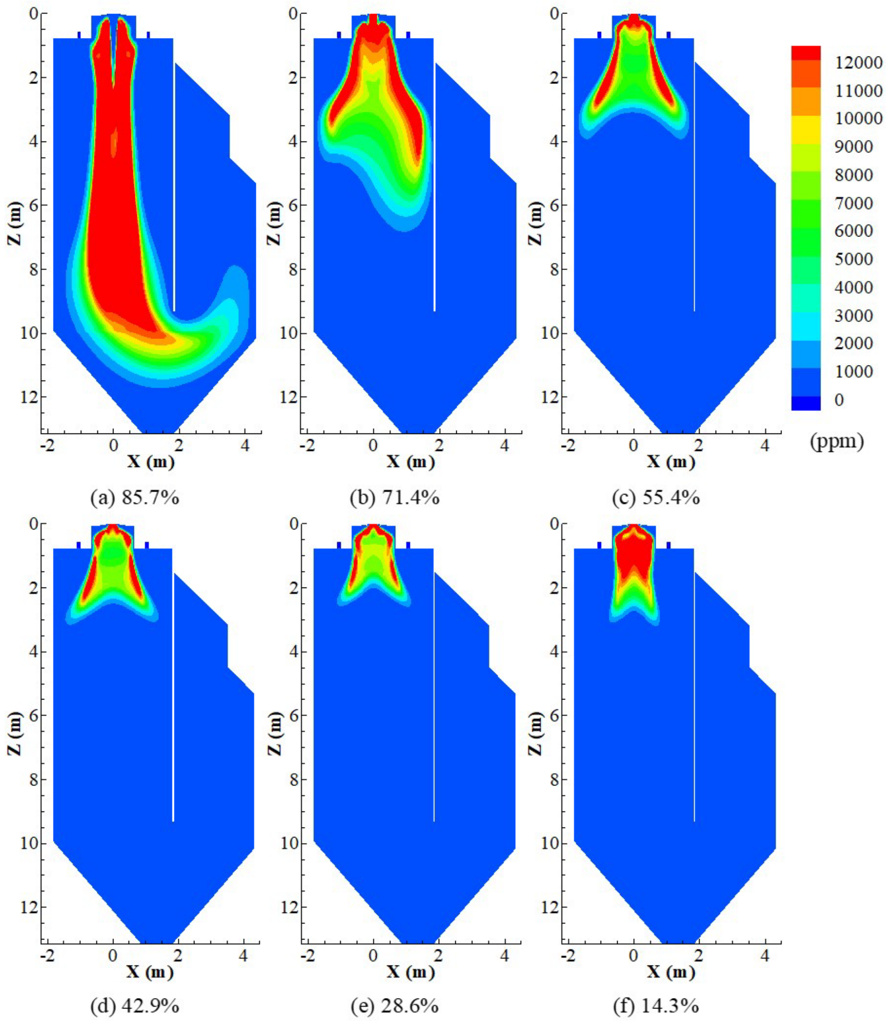

Figure 9. CO concentration contours at different separated secondary-air ratios.

Figure 10 shows the NO_X concentration distribution under different separation secondary air rates. By comparing the temperature, O_2 concentration, and CO distribution in the furnace when the separation secondary air rate is 85.7%, it can be seen that the coal powder is burned in a highly oxidizing zone at this time, which is not conducive to inhibiting NO_X formation. The high-temperature zone in the downflow furnace coincides with the high NO_X concentration zone. At the same time, due to the insufficient timely supply of the relatively large proportion of separated secondary air, the furnace is in an O_2 deficient combustion state, and the overall NO_X concentration in the furnace is still relatively low. When the separation secondary air rate is 71.4%, due to the skewed flow field in the furnace, the NO_X concentration distribution also shows a significant skew. When the separation secondary air rate decreases from 71.4% to 28.6%, the furnace temperature level continuously rises, while the mixed speed of the separated secondary air increases, and the NO_X concentration in the furnace rises accordingly. When the separation secondary air rate is 14.3%, a large amount of CO accumulates in the

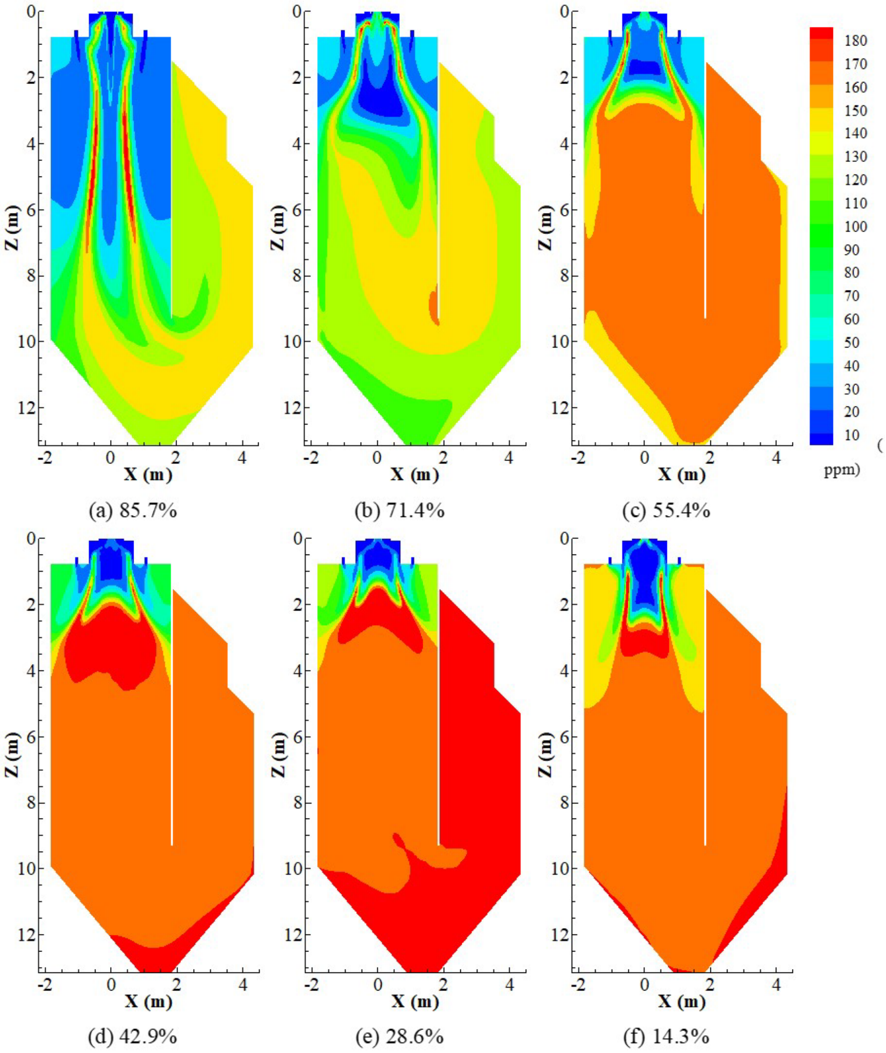

Figure 10. NO_X concentration contours at different separated secondary-air ratios.

pre-combustion chamber, and the coal powder burns in a strong reducing atmosphere.

Figure 11 presents the furnace outlet parameters under different separation secondary air rates. When the separation secondary air rate is 85.7%, the flame length inside the furnace is too long, which is not conducive to the complete combustion of coal powder. The concentration of O_2 at the outlet increases. Moreover, the excessively high exhaust gas temperature poses a threat to the safe operation of the boiler and the equipment such as the tail-end dust collector. At this time, the content of combustible substances in the fly ash is significantly higher than in other conditions, reaching 24.11%. When the separation secondary air rate is between 42.9% and 71.4%, the influence of the separation secondary air rate on the three parameters except the NO_X concentration at the furnace outlet is relatively small. As the separation secondary air rate decreases from 71.4% to 28.6%, the NO_X emission concentration at the furnace outlet gradually increases. Especially due to the insufficient depth of the downward impact of the flame and the short residence time in the high-temperature zone, when the separation secondary air rate is set at 28.6%, the changes in the outlet flue gas temperature and the combustible content in the fly ash are more obvious. At this time, the combustible content in the fly ash reaches 8.82%. Due to the squeezing of the high-speed gas flow at the outlet of the premixing chamber, the flame is difficult to expand outward, affecting the complete combustion of the coal powder. When the separation secondary air rate is reduced below 28.6%, the concentration of O_2 at the outlet and the combustible content in the fly ash further increase. At the same time, burning in a strong reducing atmosphere led to a slight decrease in the NO_X emission concentration. Considering all factors comprehensively, the optimal separation secondary air rate for the boiler is 55.4%.

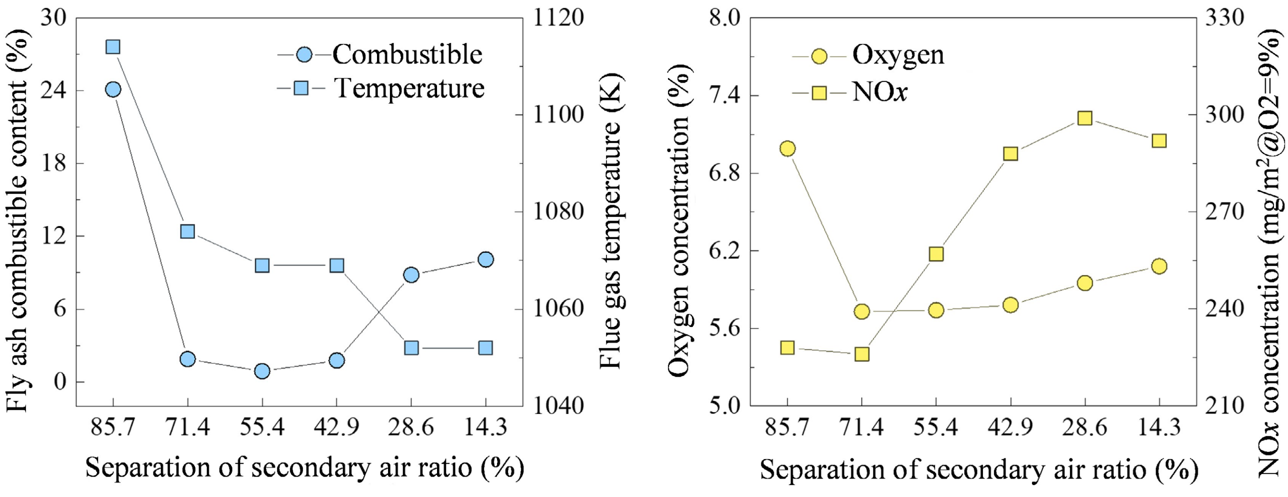

Figure 11. Effect of separated secondary-air ratio on furnace-outlet temperature, O_2, NO_X, and fly-ash combustible content.

3.2. Flue Gas Recirculation Rate

Figure 12 shows the hot-state axial velocity distribution under different flue gas recirculation ratios (Rre). With the air flow rate unchanged, increasing Rre gradually increases the gas flow rates through the outer secondary air and separated secondary air nozzles, thereby increasing the outlet velocity. As the outer secondary air flow rate increases, the swirling ability of the flow is strengthened, the amount of recirculated flue gas increases, and the region where the recirculation velocity in the central recirculation zone is greater than 5 m/s expands markedly and moves upward. Owing to the limitation of the furnace dimensions and the confinement imposed by the surrounding separated secondary air, the diameter of the central recirculation zone changes only slightly with Rre. As more flue gas participates in recirculation, the total flue-gas volume in the furnace increases, and the area with axial velocity greater than 10 m/s in the up-flow furnace increases significantly. In particular, when Rre is greater than 25%, a high-velocity region with axial velocity higher than 15 m/s appears near the rear wall of the up-flow furnace. Direct scouring of the water-cooled wall by high-speed flue gas may accelerate wall wear and is unfavorable for the long-term safe and stable operation of the boiler. Physically, this behavior is caused by the

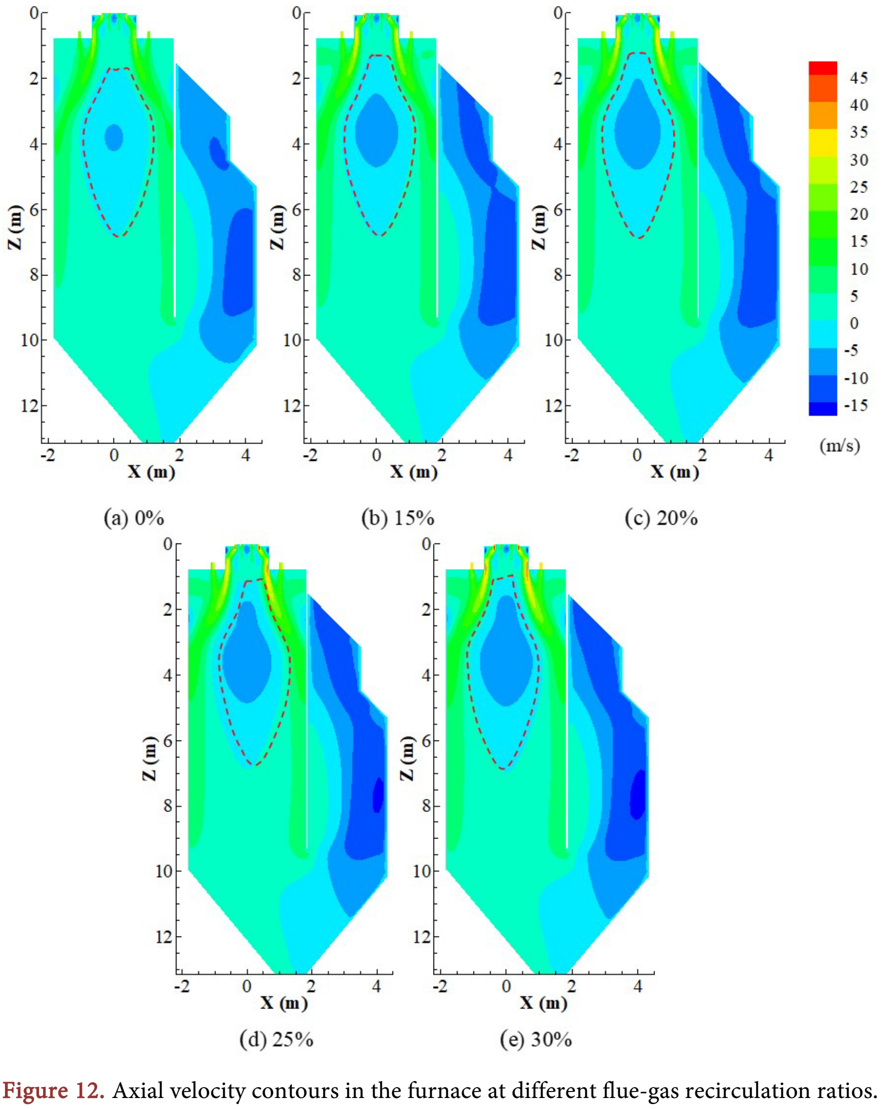

Figure 12. Axial velocity contours in the furnace at different flue-gas recirculation ratios.

increase in total jet momentum after recirculated gas is added: stronger outer-secondary-air entrainment moves the recirculation structure upward, while the confined furnace geometry limits further radial expansion.

Figure 13 shows the flue gas temperature distribution under different Rre values. Increasing the amount of recirculated flue gas has little effect on the overall flame-torch shape, but the flame size gradually decreases and the furnace filling degree is reduced. From the temperature distribution in the separated secondary air region, the downward penetration distance of the separated secondary air decreases slightly as Rre increases. This is because increasing Rre raises the flow rate and nozzle velocity of the separated secondary air, while the outer secondary air flow rate also increases, strengthening its entrainment of the separated secondary air and weakening the downward penetration capacity of the separated secondary air. The reduction in flame size is therefore attributable to the combined effects of thermal dilution by the low-temperature recirculated gas and the change in staged-jet entrainment, both of which lower the furnace temperature level and weaken flame filling.

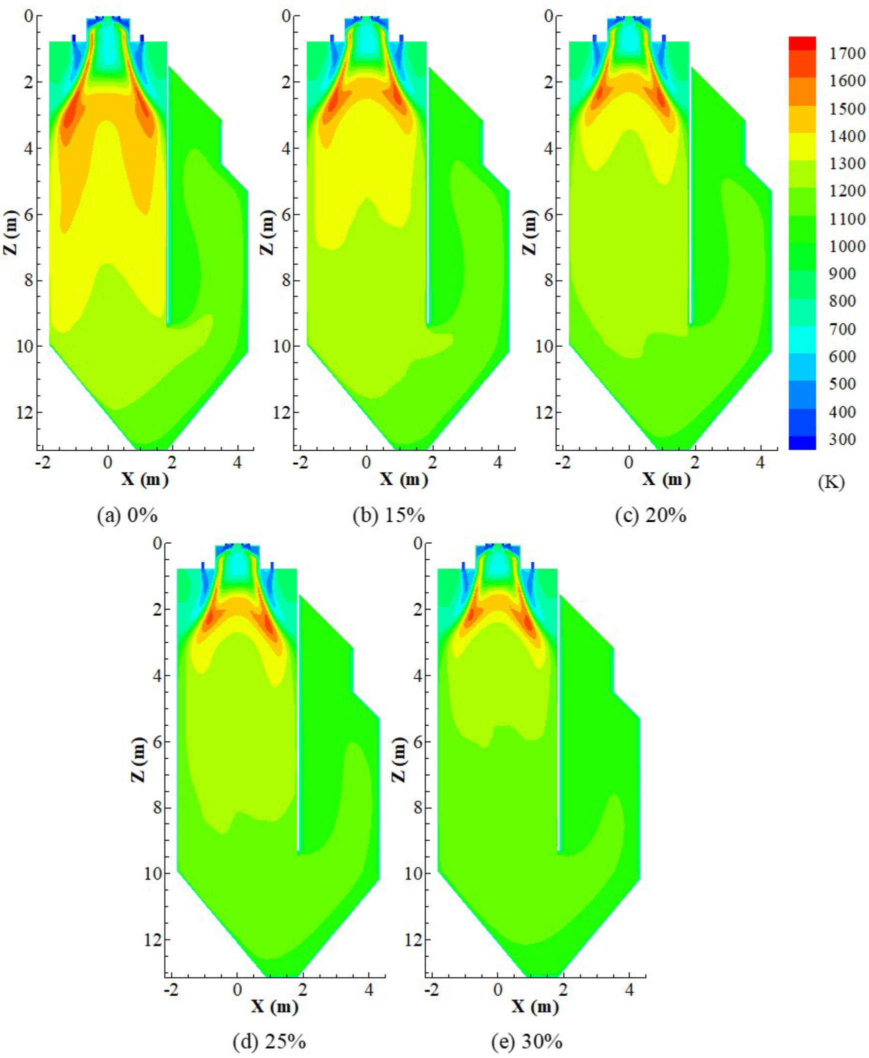

Figure 13. Furnace temperature contours at different flue-gas recirculation ratios.

Figure 14 shows the O_2 concentration distribution under different Rre values. After recirculated flue gas is mixed into the supplied air, the O_2 concentration in the burner region and near the roof of the down-flow furnace decreases markedly, especially at the bottom of the pre-combustion chamber and near the separated secondary air nozzles. However, as Rre increases, the area of the low-O_2 region in the furnace center increases instead. Meanwhile, beyond approximately 3 m from the primary air nozzle, the overall O_2 concentration in the furnace also increases with Rre. This is because the introduction of recirculated flue gas reduces the furnace filling degree of the pulverized coal flame, weakens the combustion intensity, and decreases oxygen consumption in the furnace.

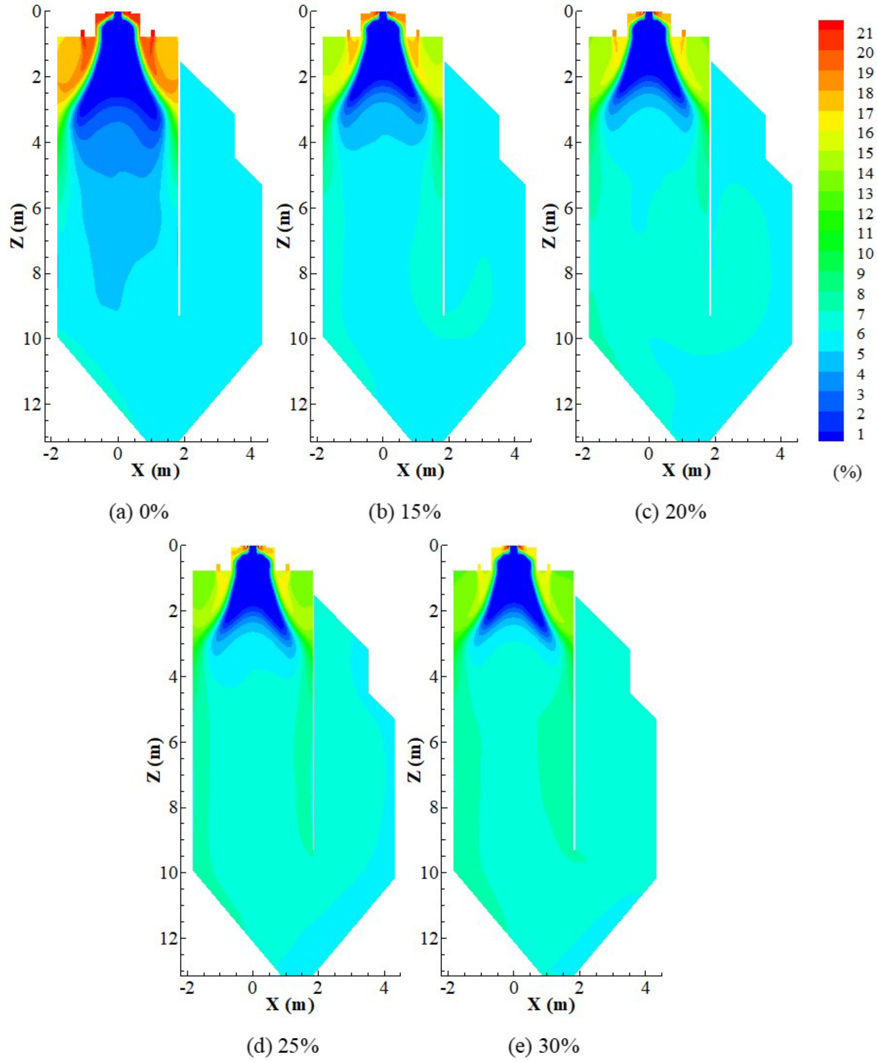

Figure 14. O_2 concentration contours at different flue-gas recirculation ratios.

Figure 15 shows the CO concentration distribution under different Rre values. The introduction of recirculated flue gas has little effect on the shape of the high-CO region in the furnace, but the area of this region gradually decreases as Rre increases, which is also attributed to the weakening of combustion intensity in the furnace. A comparison of the flue gas temperature, O_2 concentration, and CO concentration near the water-cooled wall of the down-flow furnace indicates that flue gas recirculation lowers the local flue gas temperature, increases the O_2 concentration, and reduces the CO concentration in this region. This lower-temperature atmosphere with reduced CO concentration is beneficial for avoiding high-temperature corrosion and slagging on the water-cooled wall of the down-flow furnace.

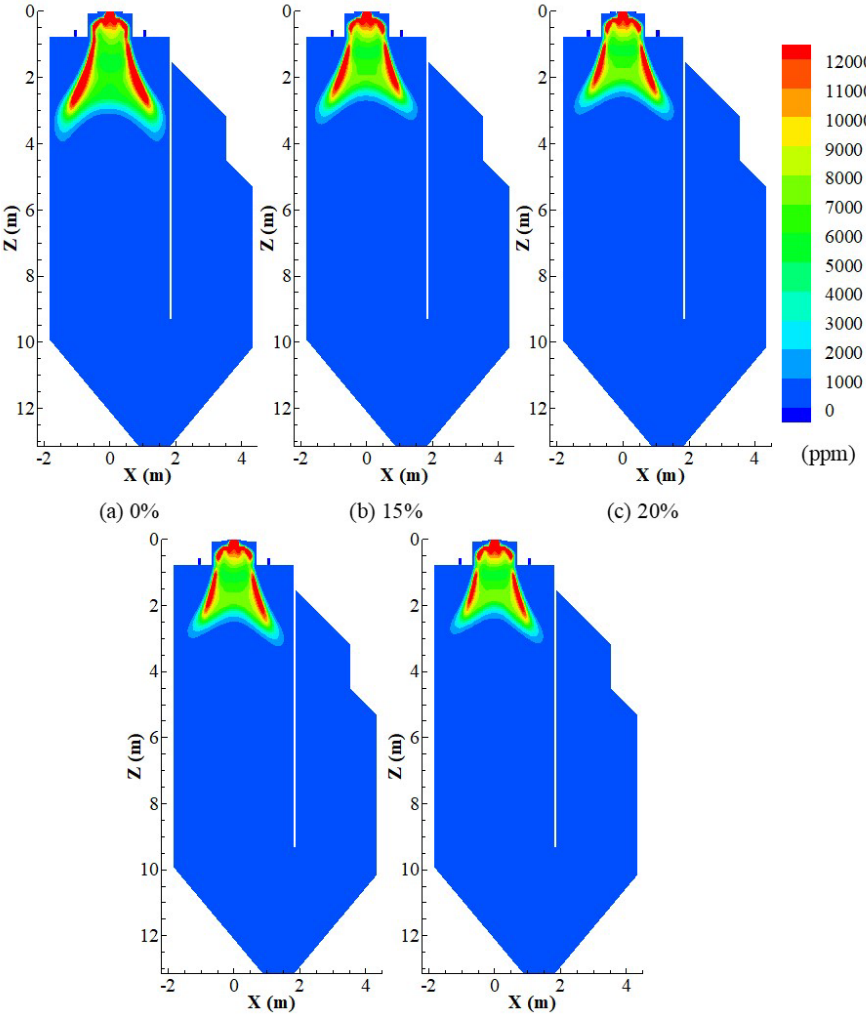

Figure 15. CO concentration contours at different flue-gas recirculation ratios.

Figure 16 shows the NO_X concentration distribution under different Rre values. Introducing low-temperature recirculated flue gas into the oxidant entering the burner not only reduces the oxygen concentration of the supplied gas, but also acts as a heat sink, thereby lowering the furnace temperature. The overall distribution in the furnace indicates that, as the amount of recirculated flue gas increases, the high-NO_X-concentration region gradually shrinks, especially in the up-flow furnace, where the NO_X concentration decreases significantly. Notably, compared with the condition without flue gas recirculation, the maximum NO_X concentration in the furnace increases after recirculated flue gas is introduced, and the high-concentration region becomes more concentrated. In the low-Rre condition, a region with NO_X concentration higher than 180 ppm appears at about 3 m from the primary air nozzle. As Rre increases, this region gradually shrinks and disappears when Rre reaches 30%. This occurs because the mixing of recirculated flue gas reduces the high-temperature area in the furnace, causing the flame to shrink and the pulverized coal to burn in a smaller space. As a result, fuel NO_X is released more locally, leading to an increase in the local NO_X concentration.

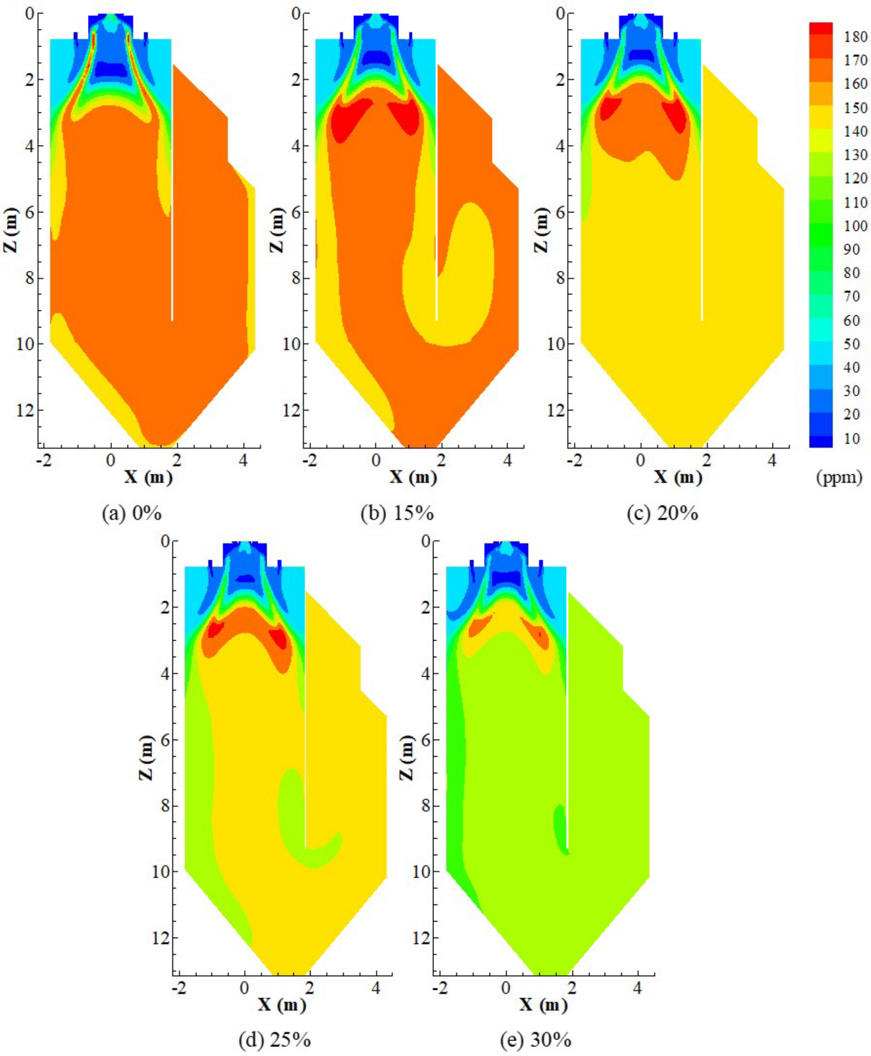

Figure 16. NO_X concentration contours at different flue-gas recirculation ratios.

Figure 17 presents the high-temperature-zone area and furnace-centerline temperature distribution under different Rre values. As Rre increases, the amount of flue gas that needs to be heated in the furnace increases, and the high-temperature area in the furnace gradually decreases. At the same time, the amount of entrained recirculated flue gas increases, and the downward penetration capacity of the separated secondary air is weakened. Therefore, with increasing Rre, the high-temperature region along the furnace centerline gradually moves upward, and the flue gas temperature along the furnace centerline beyond approximately 3 m from the primary air nozzle gradually decreases. This indicates that introducing recirculated flue gas into the boiler can effectively reduce the furnace temperature level, suppress thermal NO_X formation, and reduce the tendency for high-temperature corrosion and slagging in the furnace.

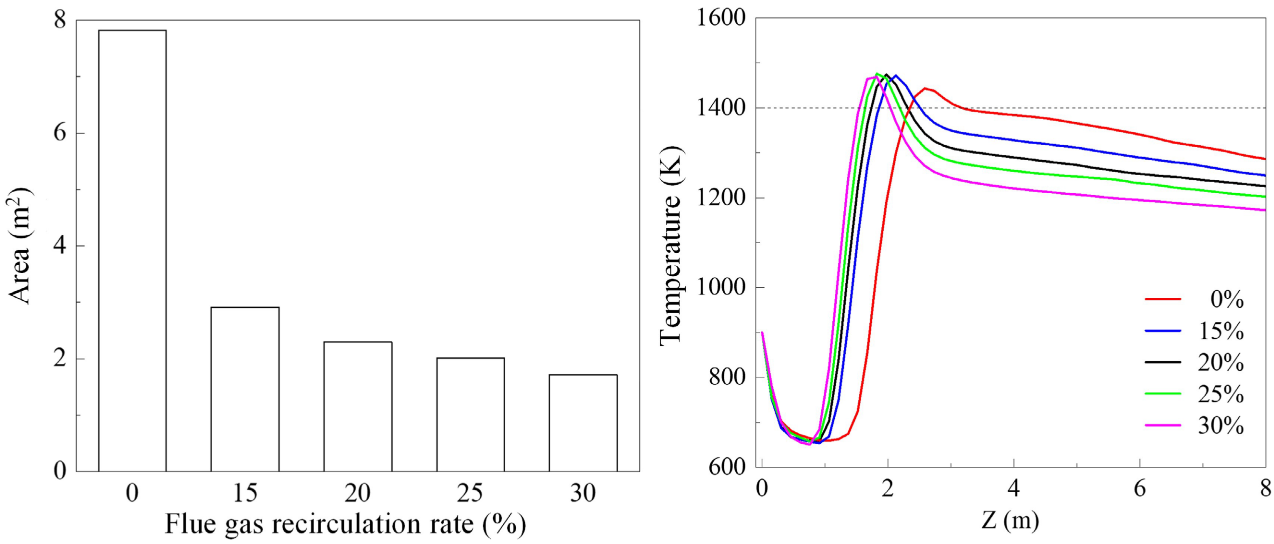

Figure 17. Effect of flue-gas recirculation ratio on high-temperature-zone area and furnace-centerline temperature.

Figure 18 shows the furnace outlet parameters under different Rre values. As Rre increases, the residence time of pulverized coal particles in the furnace becomes shorter. Meanwhile, the amount of low-temperature recirculated flue gas increases and absorbs more heat, lowering the furnace temperature. In addition, the mixing of low-O_2 recirculated flue gas reduces the oxygen concentration in the combustion region, which is unfavorable for pulverized coal combustion. Therefore, increasing Rre deteriorates the burnout of pulverized coal, decreases the exhaust gas temperature, reduces oxygen consumption, and increases the O_2 concentration at the furnace outlet. Thus, Rre should not be set too high in practical operation. In addition, when flue gas recirculation is adopted, the secondary air supply can be appropriately reduced to limit the increase in furnace outlet O_2 concentration caused by the introduction of recirculated flue gas. As Rre increases, the NO_X emission of the boiler decreases, and the reduction rate becomes faster. When Rre is set to 30%, the numerical results at the furnace outlet show that the NO_X concentration, O_2 concentration, flue gas temperature, and combustible content in fly ash decrease by 19%, increase by 0.55 percentage points, decrease by 31 K, and increase by 12.03 percentage points, respectively. Overall, when higher boiler efficiency is required, Rre should be controlled below 20% to obtain a lower combustible content in fly ash. However, when stricter outlet NO_X control is required, Rre should be set above 25% to achieve lower NO_X emissions. These quantitative changes demonstrate the principal engineering trade-off of FGR in the present boiler: stronger NO_X suppression is obtained at the cost of lower temperature and poorer burnout as Rre increases.

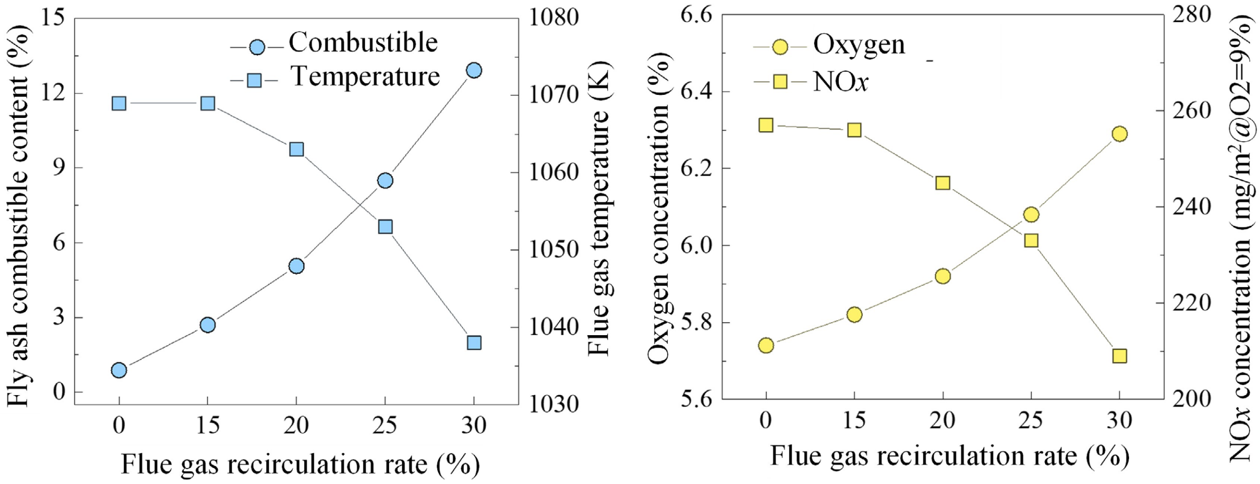

Figure 18. Effect of flue-gas recirculation ratio on furnace-outlet temperature, O_2, NO_X, and fly-ash combustible content.

The quantitative optimum values obtained in this study are specific to the investigated 29 MW boiler, the full-load condition, the tested coal, and the present burner/furnace geometry, and they should not be transferred directly to other boilers without verification. The CFD framework also contains practical engineering simplifications, including prototype-derived velocity-inlet conditions, a fixed inlet turbulence intensity of 10%, a fixed primary-air/particle slip coefficient of 0.8, a Rosin-Rammler representation of the coal-particle size distribution, a −50 Pa pressure outlet, and the P-1 radiation approximation. In addition, the underprediction of trace-level CO indicates that the simplified combustion chemistry has limited accuracy for very low CO concentrations. These limitations should be considered when applying the recommended operating ranges to other coal types, loads, or burner configurations.

4. Conclusion

This study numerically investigated the effects of the separated secondary-air ratio and flue-gas recirculation ratio on the combustion characteristics of a 29 MW industrial pulverized-coal hot-water boiler at full load. The separated secondary-air ratio strongly affected the recirculation structure, flame shape, and burnout. Excessively high or low ratios weakened combustion performance, whereas 55.4% produced a more reasonable high-temperature-zone distribution and more uniform furnace heating. Increasing the flue-gas recirculation ratio shifted the central recirculation zone upward, reduced the high-temperature-zone area and flame filling degree, weakened coal burnout, and decreased NO_X emissions. Overall, a separated secondary-air ratio of 55.4% is recommended for the investigated boiler. The flue-gas recirculation ratio should remain below 20% when combustion efficiency and burnout are prioritized, but above 25% when NO_X reduction is the main objective. These recommended values are case-specific and require validation before application to other coal types, loads, or boiler configurations.

Funding

This work was supported by the CR Power Technology R&D Program (Grant No. CRP-R&D-LX-2025-031).

Data Availability Statement

All relevant data are within the paper.

Author Contributions

Conceptualization, Leikai Deng; methodology, Leikai Deng; software, Tinghui Huang; validation, Tinghui Huang; formal analysis, Leikai Deng; investigation, Rong Yan and Zhongyan Wang; resources, Rong Yan and Zhongyan Wang; data curation, Rong Yan and Zhongyan Wang; writing—original draft preparation, Leikai Deng; writing—review and editing, Leikai Deng and Tinghui Huang; visualization, Xin Zhang; supervision, Xin Zhang; project administration, Leikai Deng; funding acquisition, Leikai Deng. All authors have read and agreed to the published version of the manuscript.

Conflicts of Interest

The authors declare no conflict of interest.

References

[1] National Bureau of Statistics of China (2021) Statistical Communique of the People's Republic of China on the 2020 National Economic and Social Development.

[2] Wang, S.M. (2020) Thoughts on the Dominant Energy Status of Coal and Green Mining in China. *China Coal*, No. 2, 11-16. (In Chinese)

[3] Liu, R., Chen, L.L., Zhao, Y.J. and Liu, M. (2017) Analysis on Effects of Energy Efficiency Regulations & Standards for Industrial Boilers in China. *IOP Conference Series: Earth and Environmental Science*, **94**, Article ID: 012147. https://doi.org/10.1088/1755-1315/94/1/012147

[4] Han, Y.F., Shen, B. and Zhang, T. (2017) A Techno-Economic Assessment of Fuel Switching Options of Addressing Environmental Challenges of Coal-Fired Industrial Boilers: An Analytical Work for China. *Energy Procedia*, **142**, 3083-3087. https://doi.org/10.1016/j.egypro.2017.12.448

[5] State Administration for Market Regulation (2019) Notice on Strengthening Energy Conservation and Environmental Protection of Boilers. (In Chinese) https://www.samr.gov.cn/tzsbj/zcfg/gfxwj/art/2018/art_c5b8fc90fefb4270975d3b81f520c899.html

[6] Yue, T., Wang, K., Wang, C., Tong, Y., Gao, J., Zhang, X., *et al.* (2020) Emission Characteristics of Hazardous Atmospheric Pollutants from Ultra-Low Emission Coal-Fired Industrial Boilers in China. *Aerosol and Air Quality Research*, **20**, 877-888. https://doi.org/10.4209/aaqr.2019.10.0531

[7] Yang, Y.M., Li, J. and He, H. (2018) Research and Proposal on Selective Catalytic Reduction Reactor Optimization for Industrial Boiler. *Journal of the Air & Waste Management Association*, **68**, 737-754. https://doi.org/10.1080/10962247.2017.1370399

[8] Zhang, Q., Yi, H.N., Yu, Z., Gao, J., Wang, X., Lin, H., *et al.* (2018) Energy-Exergy Analysis and Energy Efficiency Improvement of Coal-Fired Industrial Boilers Based on Thermal Test Data. *Applied Thermal Engineering*, **144**, 614-627. https://doi.org/10.1016/j.applthermaleng.2018.08.069

[9] Chen, B., Ye, X., Shen, J., Wang, S., Deng, S. and Yang, J. (2021) Investigations on the Energy Efficiency Limits for Industrial Boiler Operation and Technical Requirements—Taking China's Hunan Province as an Example. *Energy*, **220**, Article ID: 119672. https://doi.org/10.1016/j.energy.2020.119672

[10] Niu, F. (2020) Experimental Study on Air-Staged Combustion of 58 MW Pulverized Coal Industrial Boiler. *Clean Coal Technology*, **26**, 127-133. (In Chinese) https://doi.org/10.13226/j.issn.1006-6772.20053001

[11] Song, M.H., Huang, Y., Huang, Q., *et al.* (2021) Discussion on Low-Load Stable Combustion Technology of Swirl Pulverized Coal Burners. *Proceedings of the CSEE*, **41**, 4552-4566. (In Chinese) https://doi.org/10.13334/j.0258-8013.pcsee.210311

[12] Sun, G.G., Che, D.F. and Chi, Z.H. (2012) Effects of Secondary Air on Flow, Combustion, and NO_X Emission from a Novel Pulverized Coal Burner for Industrial Boilers. *Energy & Fuels*, **26**, 6640-6650. https://doi.org/10.1021/ef301043x

[13] Song, M.H., Huang, Q., Niu, F. and Li, S. (2020) Recirculating Structures and Combustion Characteristics in a Reverse-Jet Swirl Pulverized Coal Burner. *Fuel*, **270**, Article ID: 117456. https://doi.org/10.1016/j.fuel.2020.117456

[14] Li, G.L., Wang, N.J. and Xiao, C.W. (2015) Numerical Simulation Study on Flue Gas Recirculation in Pulverized Coal Industrial Boilers. *Clean Coal Technology*, **21**, 125-128, 133. https://doi.org/10.13226/j.issn.1006-6772.2015.02.029

[15] Wang, P.T., Wang, N.J. and Cheng, X.L. (2018) Numerical Simulation Study on Deep Air Staging in Pulverized Coal Industrial Boilers. *Clean Coal Technology*, **24**, 68-76. https://doi.org/10.13226/j.issn.1006-6772.18051402

[16] van der Lans, R.P., Glarborg, P. and Dam-Johansen, K. (1997) Influence of Process Parameters on Nitrogen Oxide Formation in Pulverized Coal Burners. *Progress in Energy and Combustion Science*, **23**, 349-377. https://doi.org/10.1016/s0360-1285(97)00012-9

[17] Fan, W.D., Lin, Z.C., Kuang, J.G. and Li, Y. (2010) Impact of Air Staging along Furnace Height on NO_X Emissions from Pulverized Coal Combustion. *Fuel Processing Technology*, **91**, 625-634. https://doi.org/10.1016/j.fuproc.2010.01.009

[18] Li, Z.Q., Chen, Z.C. and Zeng, L.Y. (2020) Swirl and W-Flame Pulverized Coal Combustion Technology: Volume I. Science Press.

[19] Chen, Z.C., Li, Z.Q., Jing, J.P., Chen, L., Wu, S. and Yao, Y. (2009) Study on Flow Fields of Centrally Fuel Rich Swirl Burner and Its Applications. *Korean Journal of Chemical Engineering*, **26**, 1186-1193. https://doi.org/10.1007/s11814-009-0216-5

[20] Zhou, C.Y., Wang, Y.Q., Jin, Q.Y., Chen, Q. and Zhou, Y. (2019) Mechanism Analysis on the Pulverized Coal Combustion Flame Stability and NO_X Emission in a Swirl Burner with Deep Air Staging. *Journal of the Energy Institute*, **92**, 298-310. https://doi.org/10.1016/j.joei.2018.01.006

[21] Echi, S., Bouabidi, A., Driss, Z. and Abid, M.S. (2019) CFD Simulation and Optimization of Industrial Boiler. *Energy*, **169**, 105-114.

https://doi.org/10.1016/j.energy.2018.12.006

[22] Liu, X., Ge, Y., Qi, G. and Zhang, S. (2019) Review of Simulation Research on Pulverized Coal Combustion in Industrial Boilers. *IOP Conference Series*: *Earth and Environmental Science*, **295**, Article ID: 052028. https://doi.org/10.1088/1755-1315/295/5/052028